ELSEVIER

Marine Geology 146 (1998) 115–135

MARINE GEOLOGY
INTERNATIONAL JOURNAL OF MARINE GEOLOGY, GEOCHEMISTRY AND GEOPHYSICS

The effect of sea breeze on beach morphology, surf zone hydrodynamics and sediment resuspension

Gerhard Masselink *, Charitha B. Pattiaratchi

Centre for Water Research, University of Western Australia, Nedlands, WA 6907, Australia

Received 17 October 1996; accepted 10 September 1997

Abstract

Beach morphodynamic processes were investigated over part of a sea breeze cycle on a microtidal, low wave energy sandy beach in southwestern Australia. Prior to the onset of the sea breeze, offshore winds with speeds less than 5 m/s prevailed. During the sea breeze, alongshore winds with speeds higher than 10 m/s were experienced. The sea breeze induced pronounced changes to the nearshore morphodynamics which were similar to that of a storm event: (1) root mean square wave height increased from 0.3 to 0.5 m; (2) zero-upcrossing wave period decreased from 8 to 4 s; (3) mean cross-shore flows reached velocities of 0.2 m/s directed offshore; and (4) the longshore current increased in strength from 0.05 to 1.0 m/s. Before the sea breeze, sediment resuspension typically occurred during isolated high-wave events associated with the passage of wave groups. Flux coupling between the wave-oscillatory currents and the suspended sediment (Jaffe, B.E., Sternberg, R.W., Sallenger, A.H., 1984. The role of suspended sediment in shore-normal beach profile changes. Proc. 19th Int. Conf. Coastal Engineering, ASCE, pp. 1983–1996) induced net onshore suspended sediment transport, resulting in beachface accretion and a steepening of the foreshore profile. In contrast, during the sea breeze, sediment resuspension was almost continuous. The suspended sediment load increased six-fold and, as a consequence, the longshore suspended sediment transport rate increased by a factor of 100. During the sea breeze, cross-shore transport was directed offshore and primarily associated with mean offshore flows. This resulted in erosion of the beachface and deposition in the surf zone and, consequently, a flattening of the beach profile. The suspended sediment load was strongly related to the Shields parameter defined for the combined action of waves and currents. Investigation of the suspended sediment profiles indicated that the degree of vertical mixing, parameterised by the sediment diffusion coefficient, increased with distance from the bed. In addition, the sediment diffusion coefficient exhibited a large temporal variation, ranging between 0.005 and 0.018 m^2/s. The variability in the sediment diffusion coefficient is possibly due to changes in the sea bed morphology.

Keywords: sea breeze; beach; suspended sediment; bedforms

1. Introduction

The afternoon sea breeze is a common—and often refreshing—feature that occurs along the majority of the world's shoreline. Together with the land breeze, the sea breeze is part of a diurnal atmospheric circulation system that arises from the contrasting thermal responses of the land and water surface because of their different thermal properties and energy balances (Abbs and Physick, 1992). The strength of this circulation is primarily

* Corresponding author. Fax: +61 93801015.
E-mail: masselin@cwr.uwa.edu.au

0025-3227/98/$19.00
PII: S0025-3227(97)00121-7

a function of the temperature difference between the air over land and that over sea (Hsu, 1988). The strongest sea breezes are therefore experienced on hot summer days in tropical and sub-tropical coastal areas. Wind velocities associated with sea breezes are generally on the order of 5 m/s, but speeds as high as 10 m/s are not uncommon (Defant, 1951). In areas where the sea breeze prevails for many months of the year, the cumulative effect of its winds on coastal processes can be considerable (Sonu et al., 1973).

The sea breeze induces changes to the incident wave field that may significantly affect beach morphology and processes. After the onset of the sea breeze, typically late morning or early afternoon, nearshore water levels and incident wave height increase, wave period decreases and wave angle may change depending on the direction of the sea breeze (Sonu et al., 1973). As a consequence, wave energy, current velocities, suspended sediment concentrations and sediment transport rates increase dramatically following the commencement of the sea breeze (Pattiaratchi et al., 1997). The change in surf zone hydrodynamics induced by the sea breeze has strong implications for beach morphology. During the sea breeze, the upper part of the beach is eroded, whereas deposition occurs on the lower part (Inman and Filloux, 1960). In addition, aeolian sand transport may occur across the berm and dunes during strong sea breeze conditions. The response of surf zone hydrodynamics and beach morphology to an increase in wave energy level at the beginning of the sea breeze is similar to that of a medium-scale storm event. Thus an investigation of the morphodynamic impacts of the sea breeze provides a small-scale analogue of medium storms on beaches.

The role of the sea breeze on beach processes and morphology is often masked by the presence of high wave energy levels and/or large tidal ranges, or further confused by a phase-coupling between the diurnal sea breeze cycle and the semi-diurnal tidal cycle (Inman and Filloux, 1960). Therefore, sea breeze effects are expected to be especially relevant in low wave energy, microtidal environments. Hegge et al. (1996) note that such environments often fail to conform to existing beach classifications and exhibit quite unique morphologies. In addition, Pattiaratchi et al. (1997) demonstrate that the surf scaling parameter, generally a good indicator of beach morphodynamic conditions in wave-dominated environments (e.g. Wright and Short, 1984), is ineffective for characterising the modal morphodynamic state of low-energy beaches that experience strong sea breezes.

The principal aims of the present study are: (1) to investigate the effect of the sea breeze on beach morphodynamics, in particular on sediment resuspension and ensuing sediment transport; and (2) to increase our understanding of sea-breeze-dominated, low wave energy beaches. To provide a theoretical framework within which to appreciate the results, some background into the sediment resuspension process is included.

2. Sediment resuspension: background

2.1. Suspended sediment profile

Numerous models are available to describe the vertical distribution of suspended sediment over the water column. One of the most commonly used—for reasons of simplicity rather than accuracy—is the diffusion model. According to this model, the upward sediment flux driven by a sediment concentration gradient is balanced by a downward flux due to the settling of sediment particles:

$$w_s \bar{c} + \epsilon_s \frac{\partial \bar{c}}{\partial z} = 0 \quad (1)$$

where w_s is the sediment fall velocity, $\bar{c}$ is the mean sediment concentration, ϵ_s is the sediment diffusion coefficient (often considered equal to the eddy viscosity of water) and $\partial \bar{c}/\partial z$ is the vertical sediment concentration gradient. The sediment diffusion coefficient is fundamental to the diffusion equation and governs the mixing of sediment particles; the larger ϵ_s, the better the sediment mixing and the smaller $\partial \bar{c}/\partial z$. The sediment diffusion coefficient varies over the water column and numerous models are available to parameterise its vertical variation (Van Rijn, 1984).

When considering time-averaged suspended sediment profiles, rather than modeling instantaneous

sediment resuspension, it may be appropriate and convenient to assume that ϵ_s is independent of z, so that Eq. (1) yields:

$$\bar{c} = C_0 \, e^{-z/l_s} \tag{2}$$

where C_0 is the reference sediment concentration at the bed and l_s is the mixing length scale given by:

$$l_s = \frac{\epsilon_s}{w_s} \tag{3}$$

Eq. (2) describes suspended sediment concentration profiles that follow a straight line when the height above the bed (z) is plotted against $\log \bar{c}$, with the sediment concentration increasing with distance from the bed. The intercept of the line ($z=0$) represents C_0 and the slope is l_s (Nielsen, 1986).

Alternatively, it may be assumed that ϵ_s increases linearly with distance from the bed (z). In that case the solution to Eq. (1) yields:

$$\bar{c} = Az^{-B} \tag{4}$$

where A and B represent empirical coefficients. Eq. (4) describes suspension profiles that follow a straight line when $\log z$ is plotted against $\log \bar{c}$. The slope of the line is proportional to B and the sediment concentration at 1 m above the bed is indicated by A.

Comparison of measured and theoretical suspension profiles with the aid of least squares analysis, enables the determination of C_0 and l_s (Eq. (2)) and A and B (Eq. (4)). Subsequently, their values can be related to hydrodynamic conditions and/or compared with theoretical predictions. Values of C_0 and A reflect the amount of sediment in the water column which is generally related to the Shields parameter (e.g. Nielsen, 1986). Parameters l_s and B describe the degree of mixing of the suspended sediment over the water column and are dependent on the sediment diffusion coefficient. The latter is related to shear stresses at the bed (Beach and Sternberg, 1988).

2.2. Bed shear stresses and Shields parameter

The amount of sediment in suspension is related to the shear stress exerted on the sea bed by the fluid. The total shear stress is composed of a skin friction component (caused by sand grains) and a form drag component (caused by bedforms). Here, only the skin friction shear stress will be considered since this component is the most important for sediment entrainment and resuspension.

Under unidirectional steady currents, the time-averaged shear velocity or friction velocity (u_{*c}) is related to the mean current velocity ($\bar{U}$) through a current friction factor (f_c) according to (Van Rijn, 1990):

$$u_{*c}^2 = \tfrac{1}{8} f_c \bar{U}^2 \tag{5}$$

with the current friction factor defined as:

$$f_c = 0.24 \left(\log \frac{12h}{k_s} \right)^{-2} \tag{6}$$

where, h is the mean water depth and k_s is the bed roughness given under flat bed conditions by $k_s = 2.5D$; and D is the mean grain size (Engelund and Hansen, 1972).

Under waves, the time-averaged shear velocity (u_{*w}) is proportional to the maximum orbital current velocity (U_m) and the wave friction factor (f_w) (Van Rijn, 1990):

$$u_{*w}^2 = \tfrac{1}{4} f_w U_m^2 \tag{7}$$

Note that Eq. (7) differs from the more conventional definition $u_{*w}^2 = 0.5 f_w U_m^2$ in which u_{*w} represents the peak shear velocity. According to linear shallow water wave theory, U_m is given by $2\sigma_u$, where σ_u is the standard deviation of the cross-shore current record. However, for irregular waves, U_m can be estimated by $2.8\sigma_u$ (e.g. Aagaard and Greenwood, 1994). The appropriateness of this formulation is demonstrated in Fig. 1. The wave friction factor can be approximated by the formula of Swart (1974) as:

$$f_w = \exp \left[5.213 \left(\frac{k_s}{a_s} \right)^{0.194} - 5.977 \right] \tag{8}$$

where a_s is the maximum bottom orbital semi-excursion ($a_s = \sigma_u T/\pi$, where T is the wave period; Wright et al., 1982).

The bed shear stress (τ_0) due to either currents or waves is related to the shear velocity according

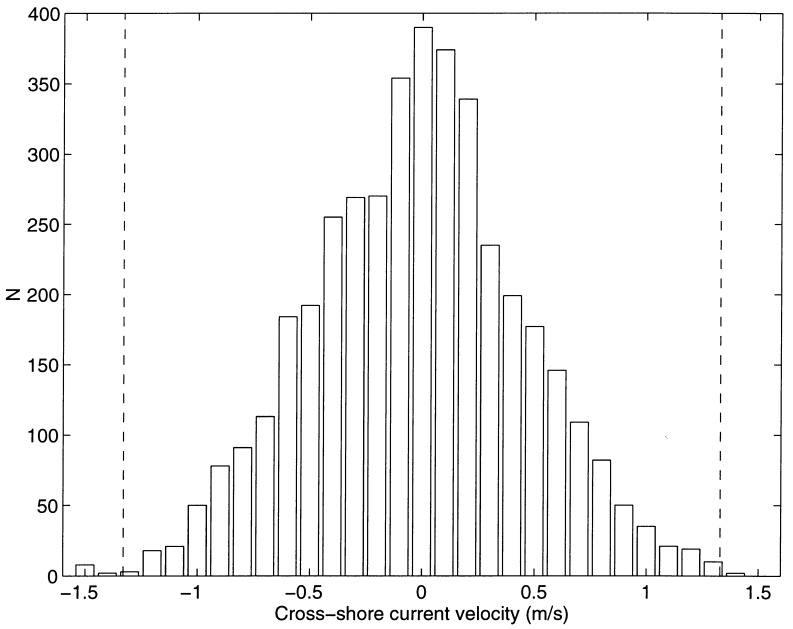

Fig. 1. Relative frequency distribution of the cross-shore current velocity for a data segment of 4096 data points. The dashed lines indicate the maximum wave orbital velocity $U_m = 1.33$ m/s estimated using 2.8 times the standard deviation of the cross-shore current record.

to:

$$\tau_0 = \rho u_*^2 \tag{9}$$

and for the combined action of waves and currents by (Beach and Sternberg, 1992):

$$\tau_0 = \rho(u_{*w}^2 + u_{*c}^2) \tag{10}$$

Alternative methods to calculate shear stresses under the combined action of waves and currents are proposed by several researchers, notably Bijker (1967) and Grant and Madsen (1979). The latter two methods are more elaborate and comparison of the resulting shear stresses determined using the present data set indicated only minor differences between the methods. The bed shear stresses were computed according to Eq. (10) and were used to calculate the Shields parameter:

$$\theta = \frac{\tau_0}{(\rho_s - \rho)gD} \tag{11}$$

where ρ_s and ρ represent the sediment and water densities, and g is the gravitational acceleration.

2.3. Suspended sediment transport calculations

Since the relatively recent development of optical back-scatterance sensors (OBS) it has become possible to collect high-resolution and high-frequency data on suspended sediment concentration, even under hostile surf zone conditions. Jaffe et al. (1984) outline the fundamental aspects involved in the calculation of suspended sediment transport using time series of suspended sediment concentration, and their approach has been followed by numerous researchers (e.g. Huntley and Hanes, 1987; Beach and Sternberg, 1988, 1992; Osborne and Greenwood, 1992a,b; Davidson et al., 1993; Russell, 1993; Aagaard and Greenwood, 1994). The following is a summary of Jaffe et al. (1984).

Consider a time series of cross-shore current velocity (u) and suspended sediment concentration (c). The product of the instantaneous velocity and the sediment concentration measured at a point gives the local instantaneous sediment transport rate (uc). The time-average of the instantaneous

sediment transport rates gives the local net sediment transport rate:

$$\langle uc \rangle = \frac{1}{n} \sum uc \tag{12}$$

where the brackets denote ensemble-averaging and n is the sample size. The velocity and sediment concentration at any instant in time are composed of a time-averaged component (overbar) and a fluctuating component (prime):

$$u = \bar{u} + u' \tag{13}$$

$$c = \bar{c} + c' \tag{14}$$

The local net sediment transport rate may also be given by:

$$\begin{aligned} \langle uc \rangle &= \langle (\bar{u} + u')(\bar{c} + c') \rangle \\ &= \bar{u}\bar{c} + \langle \bar{u}c' \rangle + \langle u'\bar{c} \rangle + \langle u'c' \rangle \end{aligned} \tag{15}$$

The terms $\langle \bar{u}c' \rangle$ and $\langle u'\bar{c} \rangle$ go to zero because by definition the time-average of the fluctuations is zero, and thus Eq. (15) reduces to:

$$\langle uc \rangle = \bar{u}\bar{c} + \langle u'c' \rangle \tag{16}$$

The term $\bar{u}\bar{c}$ is referred to as the mean sediment transport rate and is computed as the time-averaged velocity multiplied by the time-averaged sediment concentration. The term $\langle u'c' \rangle$ is the oscillating sediment transport rate and is also known as the 'flux coupling'. The oscillating transport rate may be obtained either through subtracting the mean from the net transport rate ($\langle u'c' \rangle = \langle uc \rangle - \bar{u}\bar{c}$) or by integration across all frequencies the co-spectrum between current velocity and sediment concentration (Huntley and Hanes, 1987).

The above discussion equally applies to longshore current velocities (v). However, Sternberg et al. (1984), Hanes and Huntley (1986), and Beach and Sternberg (1992) concluded that the fluctuating components of longshore velocity and sediment transport concentration were not correlated; $\langle v'c' \rangle = 0$. Consequently, the mean longshore transport rate can be calculated as:

$$\langle vc \rangle = \bar{v}\bar{c} \tag{17}$$

which is simply the product of the mean suspended sediment concentration and the mean longshore velocity.

3. Methodology

The field survey was conducted on the 23rd of January, 1992, at North City Beach, within the Perth metropolitan area, Western Australia (Fig. 2). During the survey, data were collected on: (1) beach morphology; (2) wind speed and direction; (3) beach water table; (4) instantaneous shoreline; and (5) nearshore water surface elevation, current velocity and suspended sediment concentration. The data on the beach water table and the instantaneous shoreline will not be discussed in this paper. The aim of the field survey was to monitor beach morphology, surf zone hydrodynamics and sediment suspension for a complete sea breeze cycle (24 h). However, above-average sea breeze conditions during the survey, with wind speeds exceeding 10 m/s created extremely energetic surf zone conditions. Hence, measurements were limited to only part of the sea breeze cycle (8 h).

At the start of the survey period, North City Beach was characterised by pronounced beach cusp morphology with a cusp spacing of 30 m. The beachface consisted of medium to coarse, well-sorted sand ($D = 0.5$ mm). The survey line was established across the steep-gradient (5.7°) cusp horn (Fig. 3). An array of steel pegs were inserted in the beach at 2 m intervals, extending from the top of the berm to the base of the beachface. The elevation of the nearshore profile and the survey pegs was measured using standard survey techniques. The elevation of the peg tops was assumed to remain constant and the height of the pegs above the beach was measured every 30 min.

Wind speed and direction were measured at 30 s intervals using a standard weather station deployed at 4 m height, located just landward of the berm at the southern end of the survey area. The data were later reduced to 5 min. Data on nearshore waves, currents and suspended sediment concentrations were collected using the 'S-probe', an instrument package consisting of a pressure sensor,

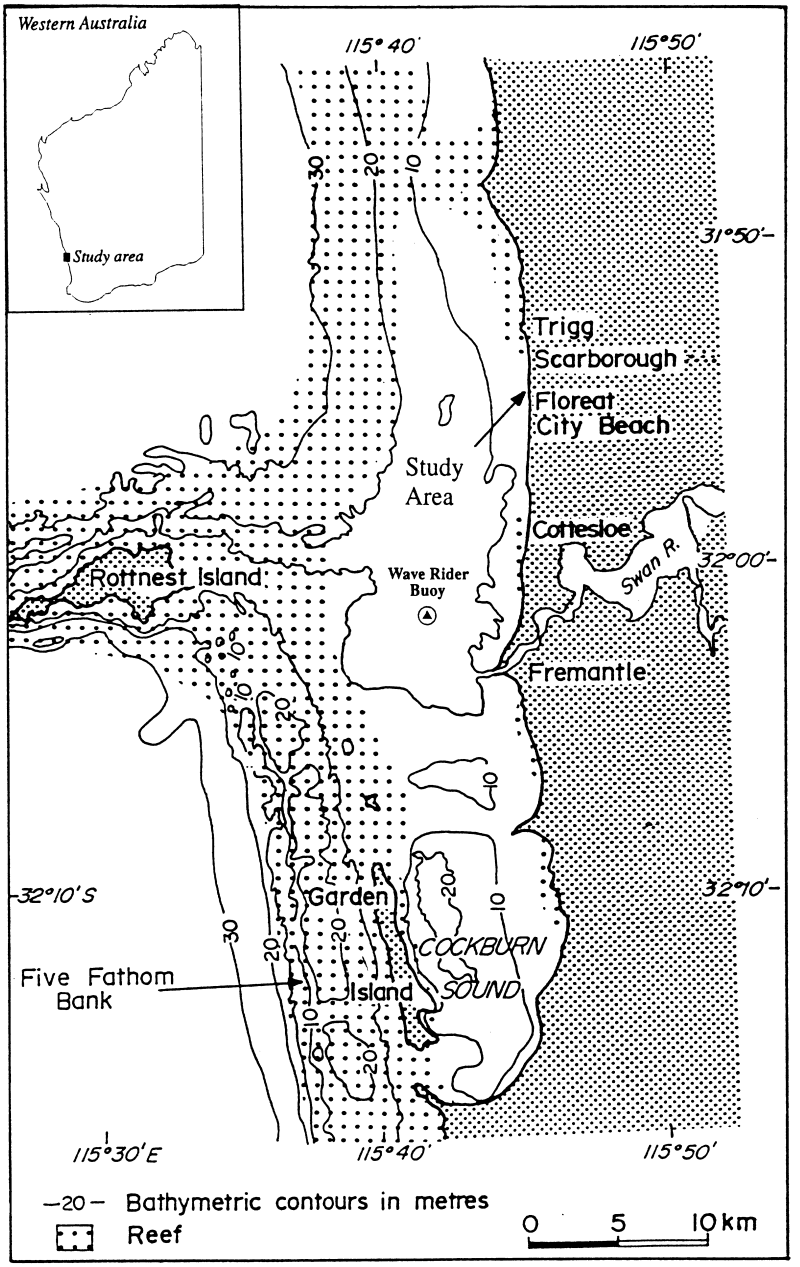

Fig. 2. Location map.

an acoustic current meter and three optical backscatterance sensors. The pressure sensor was mounted 0.35 m from the sea bed, whereas the two-dimensional, horizontal current velocity was recorded 0.2 m above the bed. The optical backscatterance (OBS) sensors measured the suspended sediment concentration at 0.025 m, 0.125 m and 0.275 m from the bed. The data were transferred via a cable connected to a shore-based computer and logged at a sampling rate of 5 Hz. The S-probe

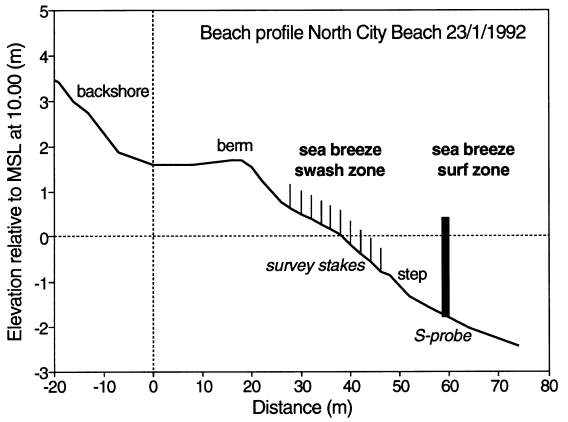

Fig. 3. Instrument deployment at North City Beach on 23rd January 1992.

was deployed opposite the cusp horn in a mean water depth of 1.5 m, approximately 20 m from the shoreline (Fig. 3). Small rip currents and suspension clouds were observed opposite the cusp embayment, but these are not considered to have affected the measurements conducted opposite the cusp horn. Prior to the sea breeze, only the highest incident waves, associated with wave groups, were breaking over the S-probe. During the sea breeze, however, the S-probe was predominantly under the influence of breaking waves. Four hours after the onset of the sea breeze, around 17 : 30 h, the S-probe could no longer be maintained in an upright position due to the extremely energetic surf zone conditions.

Calibration of the OBS sensors was conducted with sand samples collected at the survey site, using the methods and apparatus similar to that described by Ludwig and Hanes (1990). The sensors were calibrated for suspended sediment concentrations ranging from 0 to 10 g/l. The mean fall velocity of the sediment collected at the location of the S-probe was 0.04 m/s, which is equivalent to a mean grain size of 0.28 mm (Hallermeier, 1981). The minimum fall velocity represented in the sediment sample was 0.015 m/s, corresponding to a sediment size of 0.12 mm; hence only sand-sized material was present around the S-probe. Offset values for the OBSs were obtained from measurements conducted under clear water conditions. The acoustic current meter was calibrated in a flume, whereas the manufacturer's instructions were followed for the calibration of the other instruments (weather station, pressure sensor). The majority of the analysis of the water surface elevation, current velocity and suspended sediment concentration records were carried out on time series of 2048 points (~7 min). However, computation of the co-spectra between the current and suspended sediment concentration records was carried out using time series of 4096 points (~14 min).

4. Wind/wave climate and nearshore currents

The time series of wind speed and direction shown in Fig. 4 are typical of a southwestern Australian sea breeze cycle with weak offshore

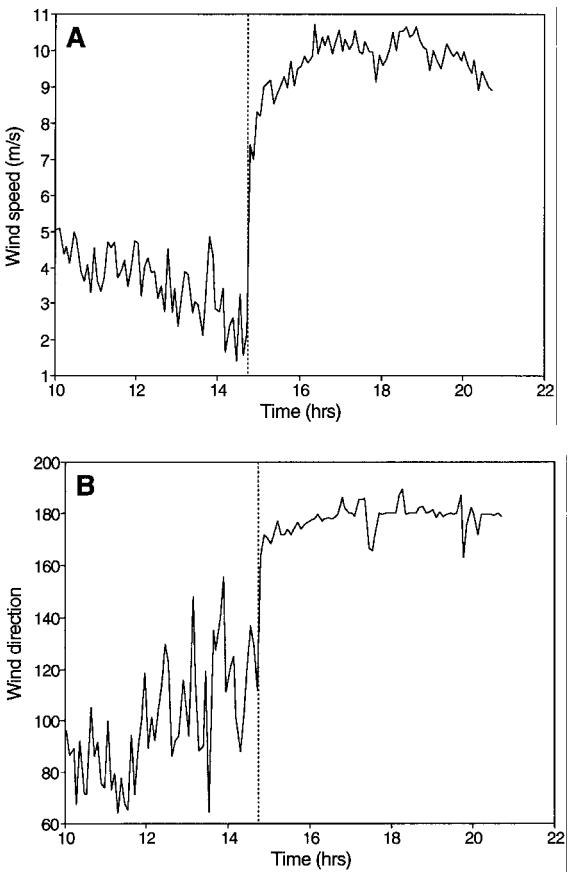

Fig. 4. Time series of: (A) wind speed; and (B) direction. The sea breeze started at 14 : 45 h.

winds in the morning and early afternoon, and a strong sea breeze starting in the afternoon and continuing into the evening. Wind speeds associated with the land breeze were less than 5 m/s, whereas the wind speeds during the sea breeze frequently exceeded 10 m/s. Such wind speeds are above average but commonly occur in the summer months on the Perth metropolitan coastline. The sea breeze started blowing at 14 : 45 h and the change in wind speed and direction was almost instantaneous. The direction of the sea breeze was consistently from the south (180°) and thus was blowing parallel to the shoreline.

The changes in the wind climate are reflected in the incident wave field and nearshore currents (Fig. 5). Prior to the sea breeze, small-amplitude swell waves with rms wave heights (H_{rms}) of 0.3 m and zero-upcrossing periods (T_z) of 7–8 s prevailed. Mean cross-shore currents were negligible (<0.05 m/s) and mean longshore currents flowed in the northward direction with velocities less than 0.1 m/s. The onset of the sea breeze induced almost immediate changes in the nearshore hydrodynamics. The wave height increased progressively, reaching 0.5 m at the end of the field survey. The wave period decreased and assumed a constant value of 4 s within 1 h of the start of the sea breeze. Offshore-directed currents in the surf zone rapidly increased in strength to 0.16 m/s and then fluctuated around 0.12 m/s. The northerly longshore current progressively increased in strength up to 1 m/s and was still increasing when the survey was abandoned.

The hydrodynamic changes observed in the surf

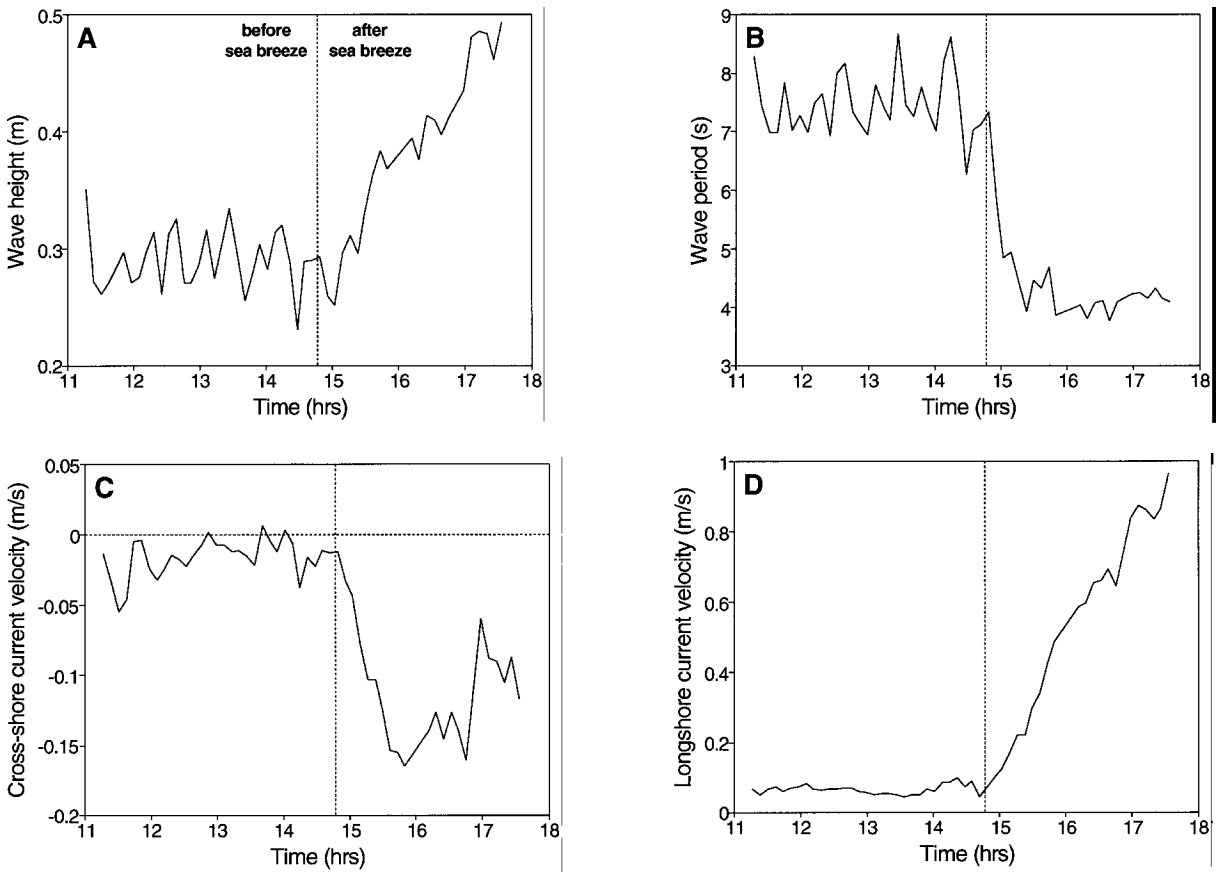

Fig. 5. Time series of: (A) rms wave height; (B) zero-upcrossing wave period; (C) mean cross-shore current; and (D) mean longshore current. The vertical dashed line indicates the start of the sea breeze.

zone can be principally attributed to the progressive addition of obliquely incident, locally generated wind waves to the shore-normal, background swell wave field (Fig. 6). The wind waves generated by the sea breeze were first noticeable at approximately 15 min after the onset of the sea breeze (15 : 00 h) with a period of 2.5 s. The wind wave period increased to a maximum of 4 s. The spectral structure of the swell energy, consisting of a 11 s peak and its first harmonic, remained relatively unchanged during the sea breeze.

5. Beach morphology

The increase in surf zone wave energy levels and nearshore current velocities induced by the sea breeze brought about significant changes to beach morphology (Fig. 7). The most conspicuous morphological effect of the sea breeze was the erosion of the cusp horn and consequent removal of the three-dimensional beach cusp morphology. Erosion of up to 0.3 m occurred on the upper part of the beachface and sediment was deposited on the lower part of the beachface and in the surf zone (Fig. 7A). Unfortunately, due to vigorous wave action, measurements of the bed level in the surf zone could not be made during the sea breeze and no information is available regarding the extent of the depositional area within the surf zone. However, around 17 : 00 h, the lower OBS sensor became covered by sediment, implying that

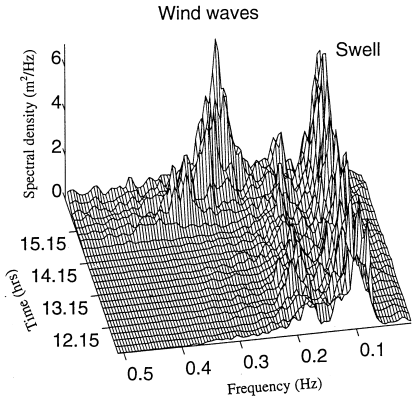

Fig. 6. Frequency–time plot of water surface elevation (after Pattiaratchi et al., 1997).

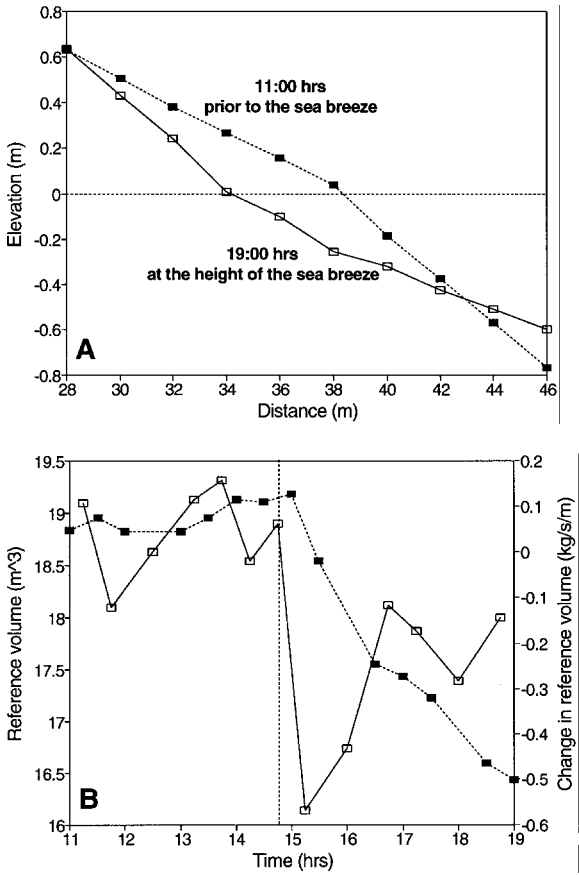

Fig. 7. (A) Beachface morphology at the start (dashed lines, solid rectangles) and the end of the survey period (solid lines, open rectangles). (B) Time series of the volume of sediment present above −0.5 m (dashed lines, solid rectangles) and the net changes in the reference volume (solid lines, open rectangles). The reference volumes and their changes have been calculated for a unit beach width. The vertical dashed line indicates the start of the sea breeze.

at least 0.03 m of accretion occurred at the mid-surf zone position. In addition, a Marsh–McBirney current meter located in the surf zone between the S-probe and the shoreline was completely buried shortly after the onset of the sea breeze, suggesting approximately 0.3 m of deposition.

The volume of sediment contained within the beachface above a reference level of −0.5 m demonstrated a slow increase in beach volume prior to the sea breeze and a rapid decrease during the sea breeze (Fig. 7B). The bed elevations at the two seaward-most stakes were not considered for

the calculation of the sediment volumes because these locations exhibited accretion during the sea breeze. Beachface accretion and steepening continued until the start of the sea breeze with onshore sediment transport rates of about 0.1 kg/s per unit beach width. These relatively low rates suggest that the beach was nearly in equilibrium with the prevailing swell conditions. Immediately after the start of the sea breeze, beachface erosion and flattening occurred with offshore sediment transport rates of around 0.5 kg/s per unit beach width. The response of the beachface to changing hydrodynamic conditions was initially rapid, but the rate of adjustment decreased during the course of the sea breeze. At the conclusion of the field survey, 4 h after the start of the sea breeze, offshore sediment transport rates were reduced to 0.2 kg/s per unit beach width. The total volume of sediment eroded from the upper beachface amounted to 2.4 m^3 over a unit beach width.

6. Suspended sediment

6.1. Suspended sediment concentration

Concomitant with the growth in nearshore energy levels was an increase in the amount of suspended sediment (Fig. 8). As the hydrodynamic conditions changed during the sea breeze, the nature and character of the sediment resuspension process varied too. Prior to the sea breeze, the suspension of sediment predominantly occurred during discrete events associated with the breaking of high waves in wave groups. During the sea breeze, however, sediment resuspension was almost continuous.

The mean suspended sediment concentration at a distance of 0.275 m from the bed (upper OBS) increased from 1 g/l in the morning to 6 g/l in the evening (Fig. 8A). This six-fold growth in sediment suspension is also apparent in the time series of the middle OBS (0.125 m from the bed), demonstrating an increase in sediment concentration from 2.5 g/l to 15 g/l (Fig. 8B). The time series of the near-bed sediment concentration ($z=0.025$ m; lower OBS) shows an even more dramatic increase in the amount of suspended sediment. In the

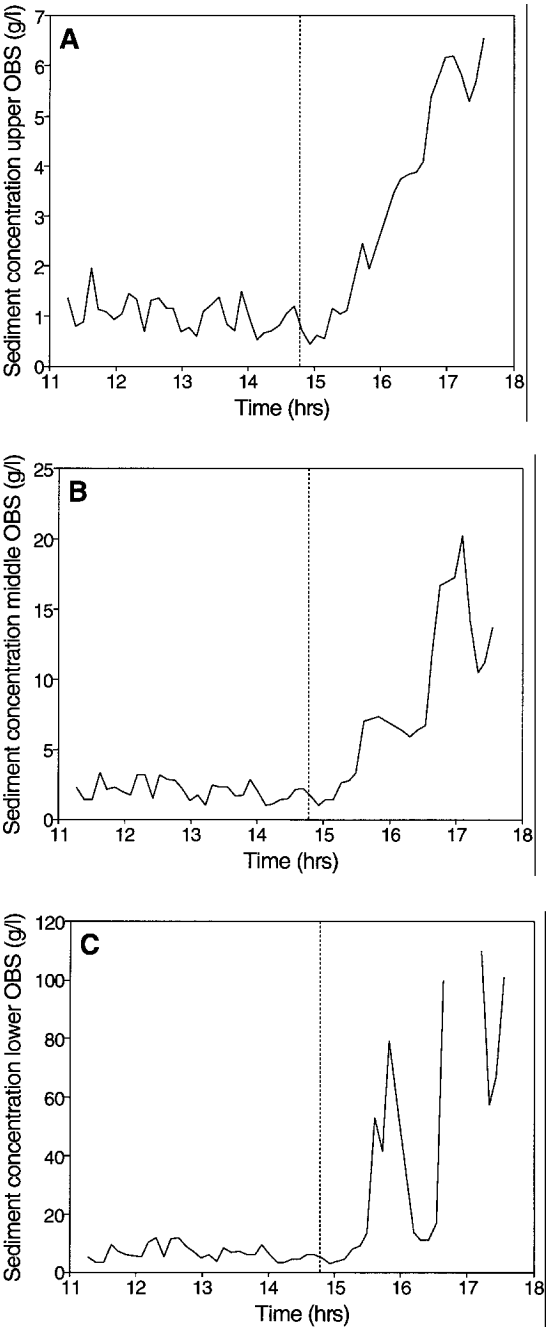

Fig. 8. Time series of suspended sediment concentrations: (A) upper OBS ($z=0.275$ m); (B) middle OBS ($z=0.125$ m); and (C) lower OBS ($z=0.025$ m). The vertical dashed line indicates the start of the sea breeze. Note the different vertical scales. Data collected by the lower OBS around 17 : 00 h are not included because of the intermittent burial of the sensor.

morning, near-bed sediment concentrations between 5 and 10 g/l were observed, but these values increased by a factor of 10 within half an hour after the onset of the sea breeze (Fig. 8C). The suspended sediment concentrations found in the present study are comparable to those reported by Beach and Sternberg (1988) for strong infragravity wave motion.

Some doubt exists, however, regarding the validity of the data collected with the lower OBS. The break in the time series at 17 : 00 h corresponds to intermittent burial of the lower OBS by sediment and for the data collected around this time the elevation of the sensor above the bed is uncertain. Observations of Black and Rosenberg (1991) indicate that sensors placed closer than 0.05 m from the bed interfere with the flow and cause sediment plumes to rise much higher above the bed than would otherwise occur. This could have resulted in unrealistically high suspended sediment concentrations recorded by the lower OBS, in particular immediately prior to and following burial. The sudden decrease in suspended sediment concentration just after 16 : 00 h also warrants further discussion. At 16 : 00 h, the S-Probe fell over, but was re-installed after several minutes. The data that were collected while the S-Probe was in a horizontal position were obviously not included in the analysis, but it is possible that the elevation of the OBS sensors above the bed for the re-installed S-Probe were different from those prior to falling over. Both the sediment concentrations measured by the lower and middle OBS exhibit a distinct drop after 16 : 00 h, indicating perhaps that the instruments were located at slightly higher elevations from the bed. Note, however, that the suspended sediment concentration measured by the upper OBS appeared to be unaffected by the re-installation of the S-probe.

6.2. Suspended sediment concentration profiles

Theoretical models of suspended sediment were compared with the field data (Fig. 9). In all instances, the power-law relationship (Eq. (4)) provided a considerably better fit than the exponential one (Eq. (2)). The small number of data points for each concentration profile precluded detailed statistical analysis of the differences in the predictive capabilities between the two theoretical models. However, the data strongly suggest that the sediment diffusion coefficient is not constant over the water column, as assumed by the exponential model, but increases away from the sea bed, at least for the lower part of the water column. It is noted that the exact elevation of the OBS sensors does not affect this conclusion since the distance between the OBS sensors remained constant during the survey.

6.3. Cross-shore suspended sediment transport

The temporal variation of the net ($\langle uc \rangle$), mean ($\bar{u}\bar{c}$) and oscillatory cross-shore suspended sediment transport ($\langle u'c' \rangle$) was computed at elevations of 0.275 m (upper OBS) and 0.125 m (middle OBS) above the bed using Eq. (16) (Fig. 10). At the upper OBS, the oscillatory component of the cross-shore suspended transport was directed onshore and the mean component was offshore. Before the sea breeze, the oscillatory transport rate was larger than the mean transport rate, resulting in a net onshore transport rate of approximately 0.1 kg m^{-2} s^{-1}. During the sea breeze, the mean transport rate exceeded that of the oscillatory transport and net offshore sediment transport rates of around 0.4 kg m^{-2} s^{-1} were attained. At the middle OBS, the pattern of net onshore sediment transport prior to the sea breeze and net offshore transport after the start of the sea breeze recurred, but the magnitudes involved were several times larger. Maximum offshore suspended sediment transport of rates 3 kg m^{-2} s^{-1} were attained around 17 : 00 h. These large rates measured by the middle OBS are partly attributed to the fact that during the sea breeze, the oscillatory component of the suspended transport was directed in the offshore direction (Fig. 10B), thereby enhancing the offshore mean transport rate.

The oscillatory component of the cross-shore sediment transport rate was subdivided into incident- and infragravity-wave components using

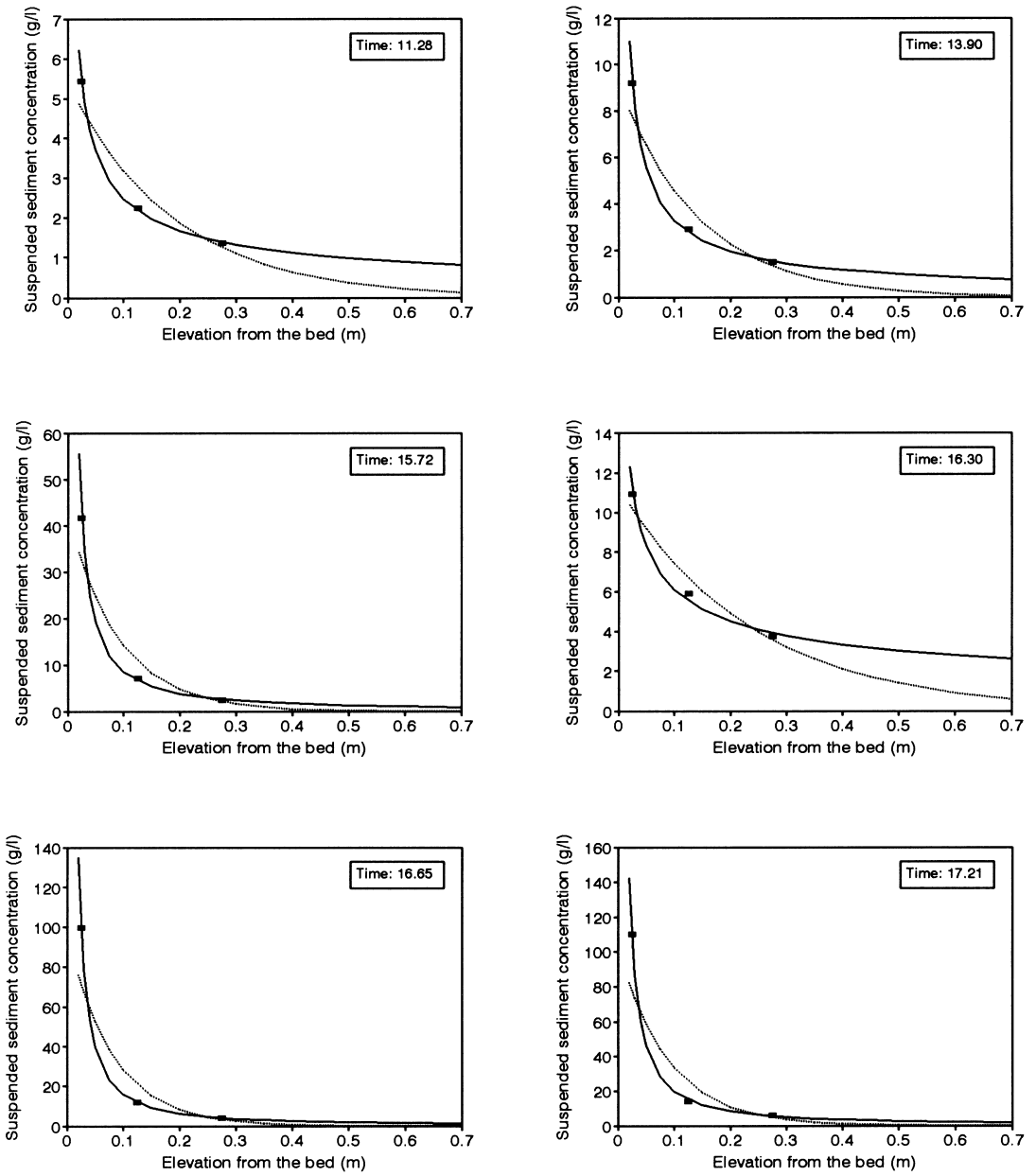

Fig. 9. Examples of vertical suspended sediment profiles with exponential (Eq. (2)) (dotted line) and power-law fit (Eq. (4)) (solid line). Note the relatively uniform suspended sediment profile at 16 : 30 h.

co-spectral analysis (Fig. 11). At the two highest elevations (middle and upper OBS), the infragravity-wave component was of less significance than the incident-wave component. At the upper OBS, the onshore sediment transport rate due to incident waves increased progressively during the sea breeze and reached values of 0.3 kg m^{-2} s^{-1}. Conversely, the sediment transport at incident wave frequencies at the middle OBS was directed offshore during the sea breeze at a rate of 1 kg m^{-2} s^{-1}.

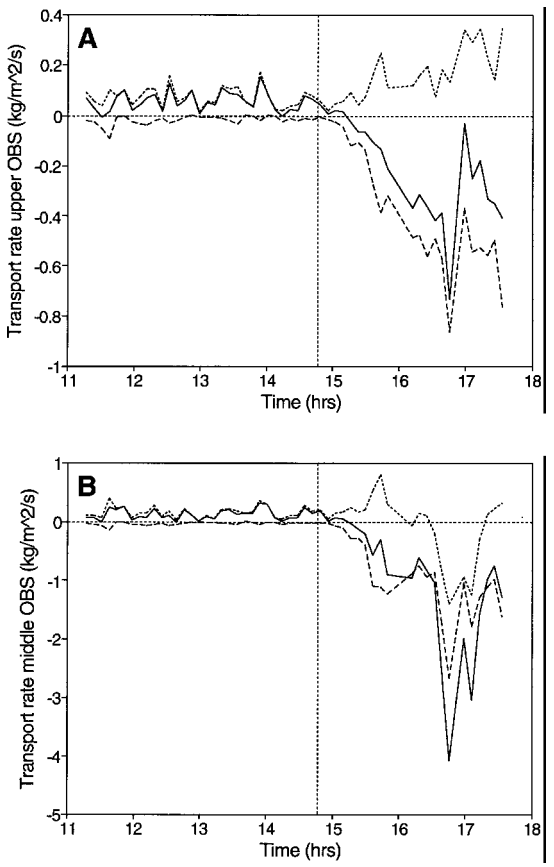

Fig. 10. Time series of cross-shore suspended sediment transport rate in kg m^{-2} s^{-1} divided into total (solid line), mean (dashed line) and oscillatory contributions (dotted line) for: (A) upper OBS ($z=0.275$ m); and (B) middle OBS ($z=0.125$ m). The vertical dashed line indicates the start of the sea breeze. Note the different vertical scales.

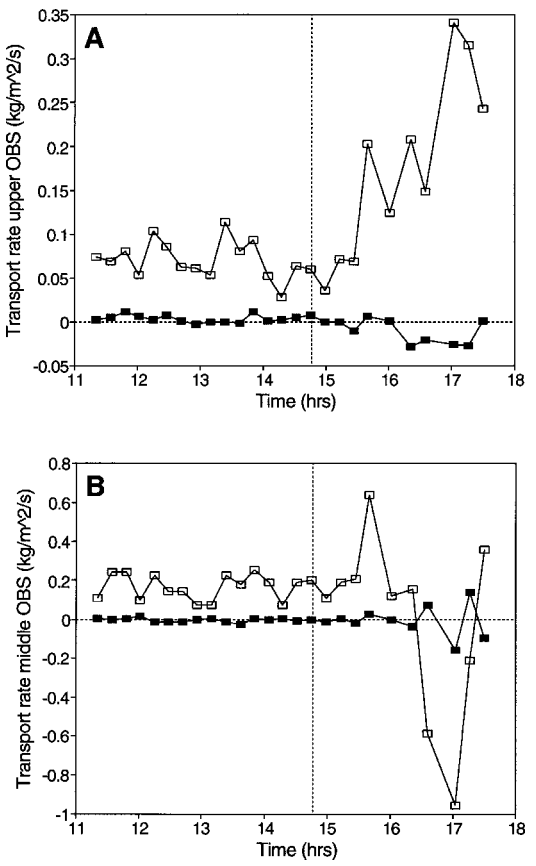

Fig. 11. Time series of cross-shore oscillatory suspended sediment transport rate in kg m^{-2} s^{-1} divided into incident- (open rectangles) and infragravity-wave contributions (solid rectangles) for: (A) upper OBS ($z=0.275$ m); and (B) middle OBS ($z=0.125$ m). The vertical dashed line indicates the start of the sea breeze. Note the different vertical scales.

6.4. Longshore suspended sediment transport

The temporal variation of the net ($\langle vc \rangle$), mean ($\bar{v}\bar{c}$) and oscillatory longshore suspended sediment transport ($\langle v'c' \rangle$) is plotted in Fig. 12 and demonstrates northerly sediment transport throughout the field survey. As observed by Sternberg et al. (1984), Hanes and Huntley (1986) and Beach and Sternberg (1992), the fluctuating components of longshore velocity and suspended sediment concentration (i.e. flux coupling) were only weakly correlated and $\langle v'c' \rangle$ was close to zero. Nevertheless, due to the obliquely incident waves, the oscillatory component of the suspended sediment transport measured by the upper OBS contributed significantly to the net longshore transport rate (Fig. 12A). During the sea breeze, net longshore transport rates were a factor of 100 larger than before the sea breeze. In addition, net longshore sediment transport rates were considerably greater than cross-shore sediment transport rates, predominantly due to the larger mean current velocities (Fig. 5C,D).

For each time series of 2048 points, the depth-integrated suspended sediment load was computed by integrating Eq. (4) over the water column using the parameters A and B obtained from least

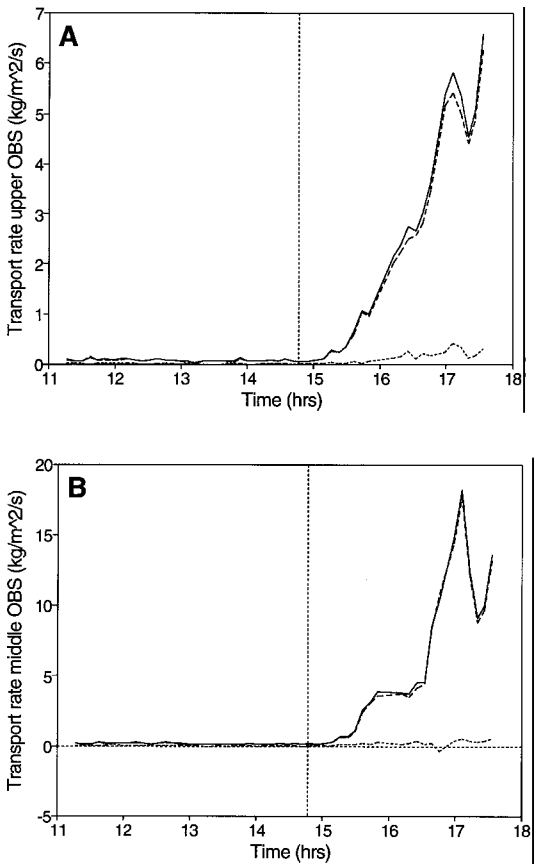

Fig. 12. Time series of longshore suspended sediment transport rate in kg m^{-2} s^{-1} divided into total (solid line), mean (dashed line) and oscillatory contributions (dotted line) for: (A) upper OBS ($z=0.275$ m); and (B) middle OBS ($z=0.125$ m). The vertical dashed line indicates the start of the sea breeze. Note the different vertical scales.

squares analysis:

$$\int_{0.01}^{h} \bar{c}\delta z = \int_{0.01}^{h} Az^{-B}\delta z = \left[\frac{A}{1-B} z^{1-B}\right]_{0.01}^{h}$$

$$= \frac{A}{1-B}\left(h^{1-B} - 0.01^{1-B}\right) \qquad (18)$$

Note that the total sediment load was calculated upward from $z=0.01$ m, rather than from the sea bed. Subsequently, the depth-integrated sediment load (in kg/m^2) was multiplied by the measured current velocity (in m/s) to obtain the depth-integrated suspended sediment transport flux (in kg m^{-1} s^{-1}). The longshore suspended sediment flux increased by a factor of 100 during the sea breeze, from approximately 0.1 kg m^{-1} s^{-1} to 10 kg m^{-1} s^{-1} (Fig. 13). The relative changes in the magnitude of the longshore sediment transport flux give an indication of the importance of the sea breeze with respect to the long-term and large-scale sediment transport patterns along the coast of southwestern Australia and other areas with strong sea breeze activity.

6.5. Modeling suspended sediment transport under waves and currents

Since both wave orbital motion and steady currents provide bottom shear stresses that may result in sediment resuspension, their relative contributions to the overall bed shear stress should be investigated. Bed shear stresses were computed using both the cross-shore and longshore components of the flow: $\sqrt{\sigma_u^2\sigma_v^2}$ was used to obtain the maximum orbital current velocity (U_m) to compute the wave shear velocity (u_{*w}; Eq. (7)) and $\sqrt{\bar{u}^2+\bar{v}^2}$ was used to determine the current shear velocity (u_{*c}; Eq. (5)).

Both wave and current shear velocities increased substantially during the field survey with the contribution of the current to the overall bed shear

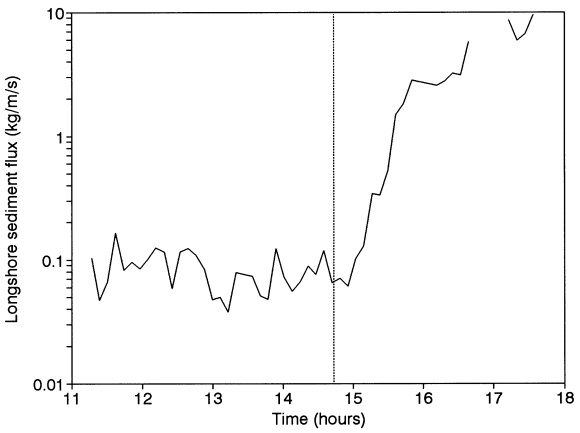

Fig. 13. Time series of vertically averaged longshore suspended sediment flux in kg m^{-1} s^{-1}. The vertical dashed line indicates the start of the sea breeze. Data collected around 17 : 00 h are not included because of the intermittent burial of the lower OBS sensor.

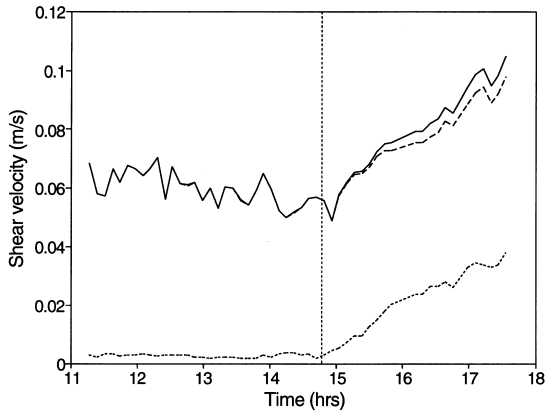

Fig. 14. Time series of total (solid line), wave (dashed line) and current bed shear velocities (dotted line). The vertical dashed line indicates the start of the sea breeze.

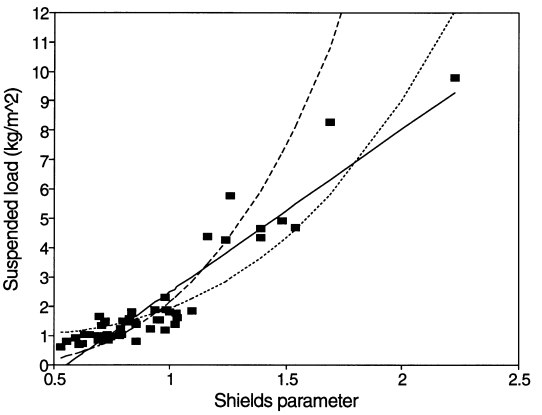

Fig. 15. Relation between Shields parameter and depth-integrated suspended sediment load. The solid rectangles indicate the data, whereas the lines represent Eq. (19a) (solid line), Eq. (19b) (dashed line) and Eq. (19c) (dotted line).

velocity of secondary importance (Fig. 14). The latter is ascribed to the larger velocities associated with the maximum wave orbital motion and the different way by which the friction factors are evaluated (Eqs. (8) and (6), respectively). It should be recognised, however, that Fig. 14 is somewhat of an oversimplification in that the wave and current contributions to the total shear stress cannot be considered separately and superimposed (Grant and Madsen, 1979). Non-linear interactions exist between the waves and currents and the sediment transport under their combined action is likely to differ from the sum of the individual contributions (Beach and Sternberg, 1992).

The amount of sediment in suspension is related to the Shields parameter via a power function (e.g. Nielsen, 1986). The depth-averaged suspended sediment concentration (Eq. (18)) and the Shields parameter (Eq. (11)) were computed and least squares analysis was used to obtain the following equations (Fig. 15):

$$\int_{0.01}^{h} \bar{c}\delta z = -3.096 + 5.567\theta_{cw} \quad r^2 = 0.87 \text{ and } n = 47 \tag{19a}$$

$$\int_{0.01}^{h} \bar{c}\delta z = -0.103 + 2.258\theta_{cw}^2 \quad r^2 = 0.89 \text{ and } n = 47 \tag{19b}$$

$$\int_{0.01}^{h} \bar{c}\delta z = -0.926 + 1.010\theta_{cw}^3 \quad r^2 = 0.84 \text{ and } n = 47 \tag{19c}$$

where θ_{cw} is the Shields parameter representing the combined influence of wave and currents. The predictive capabilities of the three equations above are not significantly different. This is primarily ascribed to the large amount of data scatter and the relatively limited range of Shields parameter values (0.5–1.5) represented in the data.

7. Discussion

It was intended to use the data from all three OBS sensors to investigate the temporal variation of C_0, l_s, A and B (Eqs. (2) and (4)) and the dependence of these parameters on hydrodynamic conditions. However, considering the uncertainties concerning the elevations of the sensors above the bed and the possibility of unrealistically high suspended sediment concentrations close to the bed due to the disturbance of the flow by the lower OBS sensor, it was felt appropriate to use only data from the middle and the upper OBS sensors ($z = 0.125$ and 0.275 m, respectively) to investigate the process of sediment resuspension in more detail.

Eqs. (2) and (3) can be combined into:

$$\epsilon_s = w_s \frac{\Delta z}{\ln \bar{c}_{upper}/\bar{c}_{middle}} \quad (20)$$

where ϵ_s is the sediment diffusion coefficient between $z=0.125$ and 0.275 m, w_s is the sediment fall velocity at the location of the S-probe ($w_s=0.04$ m/s), Δz is the elevation difference between the upper OBS and middle OBS ($\Delta z=0.15$ m), and $\bar{c}_{upper}$ and $\bar{c}_{middle}$ are the suspended sediment concentrations measured by the upper OBS and middle OBS, respectively.

The temporal variation in ϵ_s was investigated with respect to the Shields parameter for oscillatory and steady currents (θ_w and θ_c, respectively) (Fig. 16). The sediment diffusion coefficient ranges from 0.005 to 0.018 m^2/s and these values are comparable to those reported by Black et al. (1995) who collected data under similar conditions. Four major phases can be identified in the time series of the sediment diffusion coefficient (see also Fig. 8):

(A) Before the sea breeze, θ_w decreased from 0.9 to 0.7 and ϵ_s was reduced from 0.013 to 0.009 m^2/s, implying an increase in the concentration gradient and less vertical mixing. The suspended sediment concentrations measured by the middle and upper OBS sensors averaged about 2 and 1 g/l, respectively.

(B) One hour after the onset of the sea breeze, both θ_w and θ_c increased, whereas ϵ_s continued to decrease from 0.009 to 0.005 m^2/s. During the sea breeze, θ_w exceeded the value that was measured at the start of the survey. The amount of sediment in the water column increased to 7.5 g/l for the middle OBS and reached 2 g/l for the upper OBS.

(C) From 16 : 00 until 16 : 30 h, the Shields parameter continued to increase slightly; θ_w increased up to 1.4 and θ_c reached values of 0.2. Most striking is the three- to four-fold increase in ϵ_s from 0.005 to 0.018 m^2/s, indicating a dramatic improvement in the degree of sediment mixing over the water column (see also Fig. 9). The increase in ϵ_s is the result of an increase in the suspended sediment concentration a distance of 0.275 m from the bed from 2 to 4 g/l and a decrease in the concentration measured at $z=0.125$ m from 7.5 to 6 g/l. This has resulted in a more uniform suspended sediment profile indicative of improved vertical mixing.

(D) After 16 : 30 h, θ_w and θ_c progressively increased up to values of 2 and 0.35, but the degree of mixing dropped dramatically, with ϵ_s falling to 0.006 m^2/s. Suspended sediment concentrations continued to increase and attained values of around 15 and 6 g/l for the middle and upper OBS, respectively.

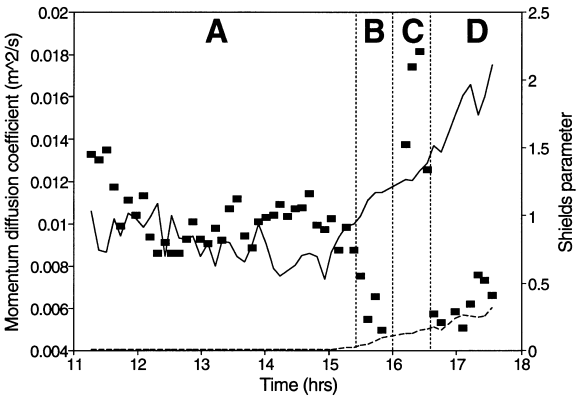

Fig. 16. Time series of the sediment diffusion coefficient (solid rectangles) and Shields parameter for waves (solid line) and currents (dashed line).

Two observations require explanation. First, the overall increase in the Shields parameter concurrent with a general decrease in the sediment diffusion coefficient during the first hour of the sea breeze. Second, the abrupt rise and fall in the sediment diffusion coefficient between 16 : 00 and 16 : 30 h. Prior to providing an explanation for these observations it is necessary to verify the reliability of the results. In particular, the following aspects need to be addressed: (1) uncertainty in sensor elevation; (2) toppling of S-probe at 16 : 00 h; (3) the role of fine material; and (4) bedform migration.

Sensor elevation: On the basis of the burial of the lower OBS sensor and the morphological changes that occurred during the sea breeze, it is inferred that an accretion of around 0.05 m has occurred from 15 : 00 to 17 : 30 h. This implies that the sediment diffusion coefficients computed using Eq. (20) and plotted in Fig. 16 represent an elevation above the sea bed ranging from 0.20 to 0.15 m. Assuming a vertically invariant diffusion

model (Eq. (2)) the elevation under consideration is irrelevant. However, it was shown in Fig. 9 that a diffusion model with sediment mixing increasing linearly with distance from the bed (Eq. (4)) was more appropriate. In addition, careful measurements conducted by Vincent and Downing (1994) using an acoustic back-scatter instrument deployed outside the surf zone demonstrate that over the lower 0.25 m of the water column, ϵ_s increases linearly with distance from the bed. According to a linear vertical distribution of ϵ_s, a decrease in elevation from 0.2 to 0.15 m will cause a decrease in ϵ_s by 25%, irrespective of a change in hydrodynamic conditions. The observed changes in ϵ_s exceed this value.

Toppling of S-probe: It is tempting to ascribe the jump in ϵ_s after 16 : 00 h to the toppling of the S-Probe at 16 : 00 h and the subsequent uncertainty regarding the elevation of the sensors above the bed. However, the difference in elevation of the OBS sensors would not have been greater than 0.05 m and can therefore not fully explain the three-fold increase in ϵ_s and the increase in sediment concentration at the upper OBS. It can, however, account for the small reduction in the suspended sediment concentration at the middle OBS.

Fines: Even at the height of the sea breeze (at the end of the survey), short spells of 'clear' water occurred as demonstrated by near-zero sediment concentrations, indicating that very fine material was not present in the water. However, it is expected that the sediment size at higher elevations is smaller than the bed material (Osborne and Greenwood, 1993). This may have resulted in a consistent over-prediction of ϵ_s. Hay and Sheng (1992) mention a decrease in the sediment size of 25% over the lower 0.3–0.4 m of the water column, equating to a decrease in the sediment fall velocity and hence an over-prediction of ϵ_s by 33% (Eq. (20)). This discrepancy is not expected to have changed much over the course of the survey.

Bedform migration: One of the reviewers suggested that the abrupt increase and subsequent decrease in ϵ_s around 16 : 00 h may be related to a migrating mega-ripple, similar to described by Osborne and Vincent (1993; their fig. 11). This is an interesting proposition that can not be wholly refuted. If a migrating mega-ripple was responsible for the sudden increase and decrease in ϵ_s, then the measurements suggest that the bedform was displaced horizontally by a full wave length in approximately 30 min. If we assume a wave length of this mega-ripple of 1 m, its migration rate is approximately 3 cm/min. This compares well with the estimate of Osborne and Vincent (1993).

In conclusion, we are of the opinion that the observed changes in the sediment diffusion coefficient are too large to be solely ascribed to the factors discussed above. Although it is possible that mega-ripple migration has played a role, we believe that modifications in the sea bed morphology has resulted in a change in the nature of the resuspension process. It is well established that the morphology of the sea bed is of fundamental importance to the resuspension process (e.g. Nielsen, 1992). Bedforms occur under distinct hydrodynamic regimes and although the boundaries that demarcate the different regimes are rather 'fuzzy', the general sequence may be represented as (Clifton, 1976; Dyer, 1986):

- Oscillatory waves: lower plane bed→rolling grain ripple→vortex ripples→upper plane bed
- Steady currents: lower plane bed→ripple→dunes→upper plane bed.

The transitions of one bedform type to the other may be described by the Shields parameter: (1) vortex ripples will be planed off and destroyed when $\theta_w > 1$ (Nielsen, 1981); (2) current ripples start forming when $\theta_c > 0.05$–0.1 (Allen, 1985; his fig. 4.26); and (3) current ripples transform to upper plane bed conditions when θ_c exceeds 0.2–0.3 (Allen, 1985; his fig. 4.26). It is recognised that the threshold values for the Shields parameter presented here are subjected to a wide range. In addition, the validity of the above threshold values under the combined action of large waves and strong currents is also questionable. Nevertheless, these values provide a basis for discussion.

It is suggested that the variations in the sediment diffusion coefficient (Fig. 16) represent four different bedform regimes. Phase A is characterised by vortex ripples in equilibrium with the long-crested swell, promoting vortex-shedding (Osborne and Greenwood, 1993) and efficient vertical mixing of sediment over the water column. During Phase

B, the vortex ripples are being planed off and eroded under the influence of increasing wave Shields parameter values. The decreasing steepness of the ripples inhibits the convection of suspended sediment high up in the water column and the suspended sediment will be confined closer to the bed, resulting in reduced sediment diffusion coefficients. During Phase C, current ripples develop under the influence of increasing longshore current velocities. The emerging current ripples provide a major roughness obstacle and vertical mixing is improved. Suspended sediment concentration is also expected to increase, as recorded by the upper OBS. During Phase D, the current velocities have increased even more, reaching the upper plane bed limit. The result is the destruction of the current ripple field leading to increased levels of sediment suspension and a decrease in the degree of vertical mixing.

Supportive evidence for the four-phase bed configuration is provided by cross-correlations between the suspended concentration measured by the lower and upper OBS sensors shown in Fig. 17. Lee and Hanes (1996) have shown that the sediment resuspension process over a rippled bed is convective, whereas diffusion is the dominant process over a plane bed. Hence, over a rippled bed, cross-correlations between suspended sediment concentration at different elevations above the bed are expected to be relatively large with maximum correlation occurring at small time lags. In contrast, cross-correlations over a plane bed will have smaller correlation coefficients and larger time lags. This is exactly what is shown in Fig. 17. The cross-correlation representing phases A (wave ripples) and C (current ripples) are very similar and characterised by a well defined and relatively high cross-correlation peak around zero time lag. In contrast, the cross-correlations representing the plane bed phases B and C have not very well defined peaks and considerable lower cross-correlation coefficients.

Unfortunately, we have not conducted field observations of the bed morphology to support our hypothesis. However, the notion that changes in the bed morphology induce modifications to the magnitude and character of sediment resuspension is not new. Bedform-related changes in sediment suspension have been reported outside the surf zone by Vincent et al. (1991) and Vincent and

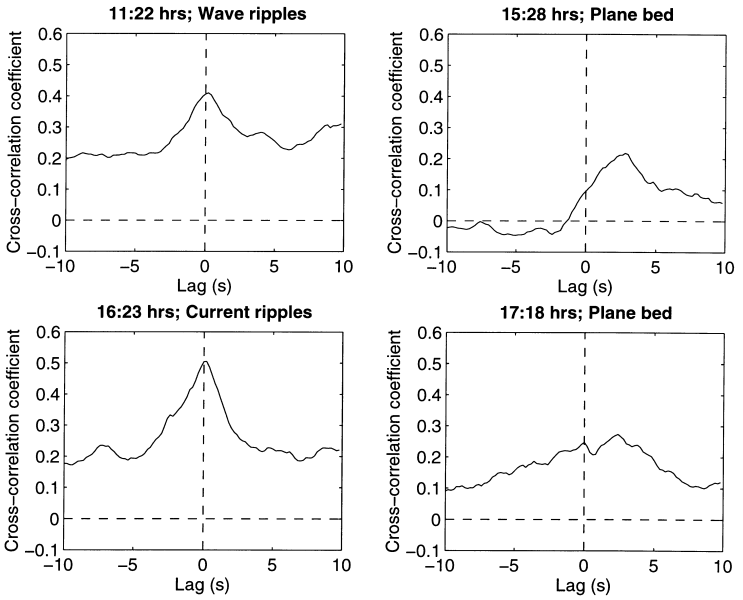

Fig. 17. Cross-correlations between suspended sediment concentration measured by the lower and upper OBS. The cross-correlations are computed using 3000 data points.

Downing (1994), and in the surf zone by Davidson et al. (1993) and Osborne and Vincent (1993).

8. Conclusions

Wind speed and direction, beach morphology, surf zone hydrodynamics and sediment resuspension were monitored over part of a sea breeze cycle. Prior to the onset of the sea breeze, offshore winds with speeds less than 5 m/s prevailed. During the sea breeze, the wind was in a longshore direction with speeds frequently exceeding 10 m/s. The change in wind speed and direction induced pronounced changes to the nearshore hydrodynamics: (1) rms wave heights increased from 0.3 to 0.5 m; (2) zero-upcrossing wave periods decreased from 8 to 4 s; (3) mean offshore-directed flows reached velocities of 0.2 m/s; and (4) the northward-flowing longshore current increased in strength from 0.05 to 1.0 m/s. Suspended sediment concentrations were measured under the combined action of incident waves and mean currents over a sea breeze cycle. All vertical suspension profiles exhibited a decrease in sediment concentration with increasing elevation. The decrease in sediment concentrations could be adequately described by a power function, implying that the sediment diffusion coefficient increases away from the bed. The depth-integrated suspended sediment load was strongly correlated with the Shields parameter.

The morphodynamic changes observed during the sea breeze cycle and discussed in the present paper are very similar to those occurring during a storm event of medium intensity in other coastal regions:

(1) Before the sea breeze, the long-period swell waves broke by plunging over a narrow surf zone or surge up the beachface, whereas during the sea breeze, the surf zone was wide and the short-period wind waves broke by plunging/spilling. Such a change in breaker type indicates a shift from reflective to more dissipative conditions that is characteristic of storms (Short, 1979).

(2) Both the nature and the magnitude of the sediment resuspension events changed in a way similar to that measured under storm conditions by Osborne and Greenwood (Osborne and Greenwood, 1992a,b). Before the sea breeze, significant sediment resuspension only occurred during isolated events under high waves associated with wave groups. During the sea breeze, however, sediment resuspension was almost continuous. The amount of sediment in the water increased six-fold during the sea breeze. This compares favourably to measurements of Kana and Ward (1980) who monitored a three- to five-fold increase in sediment concentration during a storm.

(3) The longshore suspended sediment transport rate during the sea breeze was approximately hundred times larger than before the sea breeze. This is also comparable to findings of Kana and Ward (1980) who monitored a storm-induced increase in the longshore sediment transport rate by a factor of 60.

(4) Before the sea breeze, net onshore suspended sediment transport prevailed due to the flux coupling associated with the incident waves. During the sea breeze, in contrast, net cross-shore transport was in the offshore direction and primarily associated with mean offshore flows, ie. the bed return flow or undertow. It is well established that the bed return flow provides an effective mechanism for removing sediment from the beach during storms (Roelvink and Stive, 1989).

(5) Before the sea breeze, onshore sediment transport prevailed which resulted in beachface accretion and a steepening of the beach. During the sea breeze, when offshore sediment transport occurred, the beachface was eroded. The morning after the sea breeze, the beach was almost restored to its pre-sea breeze morphology, suggesting that onshore and offshore sediment transport are balanced on a daily basis. Such a daily cycle of beach erosion and accretion is analogous to the storm cycle or the seasonal cycle of beach change (Komar, 1976).

Two important morphodynamic effects of the sea breeze on coastal processes and morphology can be identified. First, the longshore suspended sediment transport induced by the sea-breeze-generated waves and currents can be of major importance to the long-term sediment budget of the coastline. As suggested by Pattiaratchi et al. (1997), the longshore sediment transport induced by the sea breeze may account for practically all

the northward littoral drift that occurs along the Perth metropolitan coastline. Second, during the sea breeze season, beaches are continually adjusting to changing hydrodynamic conditions in an attempt to strive for equilibrium. They appear to be caught in an ongoing series of daily mini-storm cycles, characterised by erosion in the afternoon and beach accretion taking place over the rest of the day. The two-faced character of the morphodynamics of these beaches makes it impossible to define a modal or average beach morphology and inhibits application of existing beach state models (cf. Wright and Short, 1984).

Acknowledgements

We would like to thank the following people that were involved in the BREEZE92 project: Sharon Clarke, Juliet Cole, Ian and Matt Eliot, Therese Gepp, John Gould, Bruce Hegge, Ben Loffler, Matt Lyons and Tim Pearman. BREEZE92 was funded by an Individual Research grant awarded by the Division of Engineering and Computer Science at the University of Western Australia (UWA) awarded to C.P. Funding for the development of the S-probe was provided by UWA and the Centre for Environmental Fluid Dynamics. The Perth City Council is also acknowledged for granting access to the field site. Thanks also to John Boon, Bruce Hegge and John Hsu for reviewing the paper. This paper has Centre for Water Research reference ED1040 GM.

References

Aagaard, T., Greenwood, B., 1994. Suspended sediment transport and the role of infragravity waves in a barred surf zone. Mar. Geol. 118, 23–48.

Abbs, D.J., Physick, W.L., 1992. Sea-breeze observations and modelling: A review. Aust. Meteorol. Mag. 41, 9–19.

Allen, J.R.L., 1985. Principles of Physical Sedimentology. Allen and Unwin, Sydney, 272 pp.

Beach, R.A., Sternberg, R.W., 1988. Suspended sediment transport in the surf zone: response to cross-shore infragravity motion. Mar. Geol. 80, 61–79.

Beach, R.A., Sternberg, R.W., 1992. Suspended sediment transport in the surf zone: response to incident wave and longshore current interaction. Mar. Geol. 108, 275–294.

Bijker, E.W., 1967. Some considerations about scales for coastal models with movable beds. Rep. 50, Delft Hydraulics Laboratory, 142 pp.

Black, K.P., Rosenberg, M.A., 1991. Suspended sediment load at three different time scales. Proceedings Coastal Sediments '91, ASCE, pp. 313–327.

Black, K.P., Gorman, R.M., Symonds, G., 1995. Sediment transport near the break point associated with cross-shore gradients in vertical eddy diffusivity. Coastal Eng. 26, 153–175.

Clifton, H.E., 1976. Wave-formed sedimentary structures — a conceptual model. In: Davis, R.A., Ethington, R.L. (Eds.), Beach and Nearshore Sedimentation. Soc. Econ. Paleontol. Mineral. Spec. Publ. 24, 126–148.

Davidson, M.A., Russell, P.E., Huntley, D.A., Hardisty, J., 1993. Tidal asymmetry in suspended sand transport on a macrotidal intermediate beach. Mar. Geol. 110, 333–353.

Defant, F., 1951. Local winds. Compendium Meteorol. 1951, pp. 655–672.

Dyer, K.R., 1986. Coastal and Estuarine Sediment Dynamics. John Wiley, New York, 342 pp.

Engelund, F.A., Hansen, E., 1972. A Monograph on Sediment Transport. Teknisk Vorlag, Copenhagen.

Grant, W.D., Madsen, O.S., 1979. Combined wave and current interaction with a rough bottom. J. Geophys. Res. 84, 1797–1808.

Hallermeier, R.J., 1981. Terminal settling velocity of commonly occurring sand grains. Sedimentology 28, 859–865.

Hanes, D.M., Huntley, D.A., 1986. Continuous measurements of suspended of suspended sand concentration in a wave dominated nearshore environment. Cont. Shelf Res. 6, 585–596.

Hay, A.E., Sheng, J., 1992. Vertical profiles of suspended sand concentration and size from multifrequency acoustic backscatter. J. Geophys. Res. 97, 15661–15677.

Hegge, B.J., Eliot, I.G., Hsu, J., 1996. Sheltered sandy beaches of southwestern Australia. J. Coastal Res. 12, 748–760.

Hsu, S.A., 1988. Coastal Meteorology. Academic Press, New York, 260 pp.

Huntley, D.A., Hanes, D.M., 1987. Direct measurement of suspended sediment transport. Coastal Sediments '87, ASCE, pp. 723–737.

Inman, D.L., Filloux, J., 1960. Beach cycles related to tide and local wind regime. J. Geol. 68, 225–231.

Jaffe, B.E., Sternberg, R.W., Sallenger, A.H., 1984. The role of suspended sediment in shore-normal beach profile changes. Proc. 19th Int. Conf. Coastal Engineering, ASCE, pp. 1983–1996.

Kana, T.W., Ward, L.G., 1980. Nearshore suspended sediment load during storm and post-storm conditions. Proc. 17th Int. Conf. Coastal Engineering, ASCE, pp. 1158–1174.

Komar, P.D., 1976. Beach Processes and Sedimentation. Prentice-Hall, Englewood Cliffs, New Jersey, 429 pp.

Lee, T.H., Hanes, D.M., 1996. Comparison of field observations of the vertical distribution of suspended sand and its prediction by models. J. Geophys. Res. 101, 3561–3572.

Ludwig, K., Hanes, D., 1990. A laboratory evaluation of optical

backscatterance suspended solids sensors exposed to sand–mud mixtures. Mar. Geol. 94, 173–179.
Nielsen, P., 1981. Dynamics and geometry of wave-generated ripples. J. Geophys. Res. 86, 6467–6472.
Nielsen, P., 1986. Suspended sediment concentrations under waves. Coastal Eng. 10, 13–31.
Nielsen, P., 1992. Coastal Bottom Boundary Layers and Sediment Transport. Advanced Series on Ocean Engineering, Vol. 4. World Scientific, Singapore, 324 pp.
Osborne, P.D., Greenwood, B., 1992a. Frequency dependent cross-shore suspended sediment transport, 1. A non-barred shoreface. Mar. Geol. 106, 1–24.
Osborne, P.D., Greenwood, B., 1992b. Frequency dependent cross-shore suspended sediment transport, 2. A barred shoreface. Mar. Geol. 106, 25–51.
Osborne, P.D., Greenwood, B., 1993. Sediment suspension under waves and currents: Time scales and vertical structure. Sedimentology 40, 599–622.
Osborne, P.D., Vincent, C.E., 1993. Dynamics of large and small scale bedforms on a macrotidal shoreface under shoaling and breaking waves. Mar. Geol. 115, 207–226.
Pattiaratchi, C., Hegge, B.J., Gould, J., Eliot, I.G., 1997. Impact of sea breeze activity on nearshore and foreshore processes in Southwestern Australia. Continental Shelf Research, in press.
Van Rijn, L.C., 1984. Sediment transport, Part II. Suspended load transport. J. Hydraul. Eng. 110, 1613–1641.
Van Rijn, L.C., 1990. Handbook Sediment Transport by Currents and Waves. Delft Hydraulics, Rep. H461.
Roelvink, J.A., Stive, M.J.F., 1989. Bar-generating cross-shore flow mechanisms on a beach. J. Geophys. Res. 94, 4785–4800.
Russell, P.E., 1993. Mechanisms for beach erosion during storms. Cont. Shelf Res. 13, 1243–1265.
Short, A.D., 1979. Three dimensional beach-stage model. J. Geol. 87, 553–571.
Sonu, C.J., Murray, S.P., Hsu, S.A., Suhayda, J.N., Waddell, E., 1973. Sea-breeze and coastal processes. EOS, Trans. Am. Geophys. Union 54, 820–833.
Sternberg, R.W., Shi, N.C., Downing, J.P., 1984. Field investigations of suspended sediment transport in the nearshore zone. Proc. 19th Int. Conf. Coastal Engineering, ASCE, pp. 1782–1798.
Swart, D.H., 1974. A schematization of onshore–offshore transport. Proc. 14th Int. Conf. Coastal Engineering, ASCE, pp. 884–900.
Vincent, C.E., Downing, A., 1994. Variability of suspended sand concentrations, transport and eddy diffusivity under non-breaking waves on the shoreface. Cont. Shelf Res. 14, 223–250.
Vincent, C.E., Hanes, D.M., Bowen, A.J., 1991. Acoustic measurements of suspended sand on the shoreface and the control of concentration by bed roughness. Mar. Geol. 96, 1–18.
Wright, L.D., Short, A.D., 1984. Morphodynamic variability of surf zones and beaches: A synthesis. Mar. Geol. 56, 93–118.
Wright, L.D., Nielsen, P., Short, A.D., Green, M.O., 1982. Morphodynamics of a macrotidal beach. Mar. Geol. 50, 97–128.